Hindawi
Journal of Sensors
Volume 2019, Article ID 8476489, 10 pages
https://doi.org/10.1155/2019/8476489

Research Article

Design and Evaluation of a Multidirectional Thermal Flow Sensor on Flexible Substrate

Dimitris Barmpakos,[1,2] **Ioannis Th. Famelis**,[1] **Anastasios Moschos**,[1] **Damianos Marinatos**,[1] **and Grigoris Kaltsas**[1]

[1]*microSENSES Laboratory, Department of Electrical and Electronic Engineering, University of West Attica, Athens, Greece*
[2]*Institute of Nanoscience and Nanotechnology (INN), NCSR Demokritos, Athens, Greece*

Correspondence should be addressed to Dimitris Barmpakos; d.barmpakos@inn.demokritos.gr

Received 28 September 2018; Revised 20 November 2018; Accepted 10 December 2018; Published 12 February 2019

Academic Editor: Paolo Bruschi

The development and the corresponding evaluation of a multidirectional thermal flow sensor are presented in this work. The sensor was fabricated on a flexible substrate, allowing for new applications, since it provides the possibility of installation in nonplanar surfaces such as pipelines. Furthermore, the sensing elements are not in direct contact with the fluid, which increases the device reliability, extends its application range, and allows the noncontact monitoring of fluids. This was achieved by utilizing the substrate as a protective layer between the sensing elements and the fluid under measurement. The operation principle is based on the determination of the flow-induced temperature profile variations. A dedicated experimental setup was designed and used for the device evaluation. Both flow velocity value and direction were successfully extracted, while the results were consistent with the predicted theoretical values. A single-layer back propagation neural network that correlates the sensors' readouts to the angle of rotation was implemented, which leads to a mean absolute direction estimation error in the order of 2.7 degrees independent to the training procedure datasets.

1. Introduction

Determination of flow velocity and direction in harsh environments is a major concern in various applications, such as gas flow measurement in pipelines [1], meteorology [2], agricultural production [3], avionics [4] and active flow control in aviation [5], intelligent air-conditioning systems [6, 7], and wind turbine installations [8]. Flow sensors also find critical applications in biomedical fields, for example, installation in external ventricular drains [9], tracheal intubation flow sensing [10], sleep apnea monitoring [11], and blood flow sensing [12].

There are a few principles of operation suggested in the literature, such as MEMS with beam structures [13], piezoresistive sensors [11] where strain, stress, or pressure is translated into flow, or more recent multidirectional flow measurements using thermoelectric generators in effective radial topology [14]. However, thermal flow sensors are considered key technology, mainly because they are not composed of moving parts; therefore, there is no mechanical degradation over time and design and implementation require less production steps. Also, being a mature technology, challenges regarding driving electronic circuits and interfacing have been tackled.

Directional flow sensors based on thermal principles of operation [14–22] have been studied extensively since the evolvement of micromachining technology and the introduction of the first device on silicon substrate [23]. Great efforts towards minimizing energy consumption are presented in the literature [16, 21], thus allowing for applications where minimal energy footprint is required, as in wireless sensor networks [20].

Enhanced sensor performance has been demonstrated by various implementations; for instance, the addition of sensing elements at different distances from the heating element has been linked to a broader flow velocity detection

range [24, 25], while improved direction sensitivity has been achieved with the incorporation of additional heaters [26, 27]. Intelligent techniques have also been introduced in order to further improve accuracy or facilitate flow direction estimation and compensation for sensor fabrication asymmetries, such as Σ-Δ modulation [27] and Artificial Neural Networks (ANNs) [22, 28]. Also, data from directional flow sensors mounted onto different unmanned vehicles (such as drones [29]) can be used in mathematical models and algorithms [30–32] for real-time correction of operation and optimal operation.

Nevertheless, MEMS manufacturing technology presents some inherent drawbacks, such as the requirement for complicated and expensive manufacturing procedures and the relatively frail nature of rigid-substrate devices, mostly due to wire bonding connections and other packaging issues [33]. Alternative devices, based on flexible substrates and thin film technology, have been demonstrated [22, 34, 35], but they either provide solely uniaxial information of flow rate or have high error in flow angle detection.

In this work, the design and implementation of a low-cost multidirectional thermal flow sensor on flexible substrate based on previously presented preliminary results [36], with compensation via a suitable Artificial Neural Network, are presented. Measurements demonstrate that performance is comparable to corresponding silicon devices in both flow rate and flow direction detection. In addition, the sensing elements are fully isolated from the fluid; as a result, the implementation presents a robust, maintenance-free solution for harsh environments.

2. Principle of Operation

The device incorporates four orthogonally placed sensing elements (R1, R2, R3, and R4) with equal distance from a centered heater, as shown in Figure 1, allowing the determination of flow vector (both flow rate value and direction). Heater operation in constant current as well as in the constant temperature mode was evaluated for the determination of the flow rate; in the first case, the heater's resistance (which presents a linear correlation to temperature) drops as the flow rate increases, whereas in the second case, the power required to maintain a constant heater temperature is proportional to the flow rate applied. For both operating modes, appropriate electronics were utilized for supplying controllable power to the heater element.

Flow angle can be derived from the differential signals of the sensing elements due to the flow-induced heat transfer; therefore, both the flow rate and the direction can be extracted simultaneously [26].

The following functions show the correlation between the flow angle and the differential signals of the sensing elements:

$$\begin{aligned} \Delta T_x &= \Delta T_0 \cdot \cos\varphi, \\ \Delta T_y &= \Delta T_0 \cdot \sin\varphi, \\ \varphi &= \arctan\left(\frac{\Delta T_y}{\Delta T_x}\right), \end{aligned} \tag{1}$$

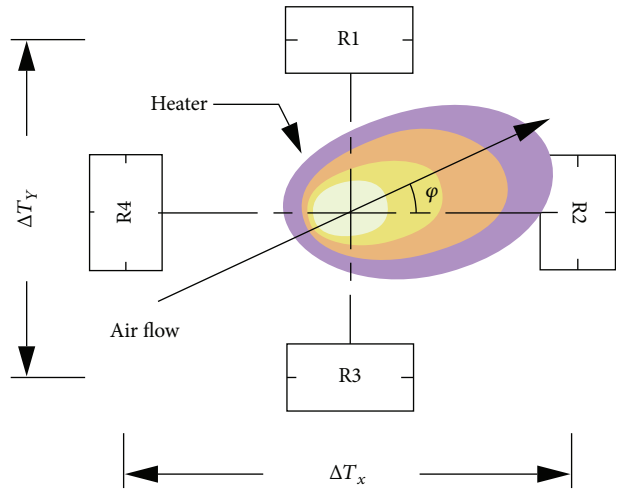

Figure 1: Sensor layout representation. ΔT_x and ΔT_y are the temperature differences measured between sensing element pairs R2-R4 and R1-R3, respectively.

where ΔT_0 represents the temperature drop induced on the sensing element pairs by the applied flow. The signs of ΔT_x and ΔT_y must be taken into account when calculating the inverse tangent in order to obtain four-quadrant results.

3. Sensor Fabrication: Experimental Setup

The fabrication procedure is compatible with standardized, low-cost flexible PCB manufacturing technology, while the components used are widely available and the entire process features a high repeatability rate.

In Figure 2, the manufacturing process is illustrated; the substrate is a 100 μm thick polyimide (PI) film, prelaminated with copper. The copper conductive traces are patterned using a typical photoresist-based process and a low-cost mask, printed on polyester film. SMT Pt100 elements (in typical 0603 package) are utilized for both heating and sensing elements. The four sensing elements are soldered at a distance of 2.5 mm from the heating element, and finally, the device is sealed with epoxy material on the upper side.

The resulting device with the corresponding housing for the evaluation setup is presented in Figures 2(c) and 2(d). The sensing elements and the heater are formed on the upper (patterned) surface of the PI film as shown in Figure 2(c). It should be underlined that flow is applied on the nonpatterned surface of the substrate. The bottom surface of the PI film is facing inside the flow channel as shown in Figure 2(d), thus offering isolation, both chemically and mechanically, from the gas/fluid flow, while permitting thermal interaction via the thin polyimide membrane. Although the sensing elements are not in direct contact with the fluid, the membrane thickness allows for thermal coupling, thus resulting in adequate sensitivity and detection range, as indicated by the corresponding results.

The measurement setup (Figure 3(a)) consisted of a specially designed plexiglass flow channel, with a suitable

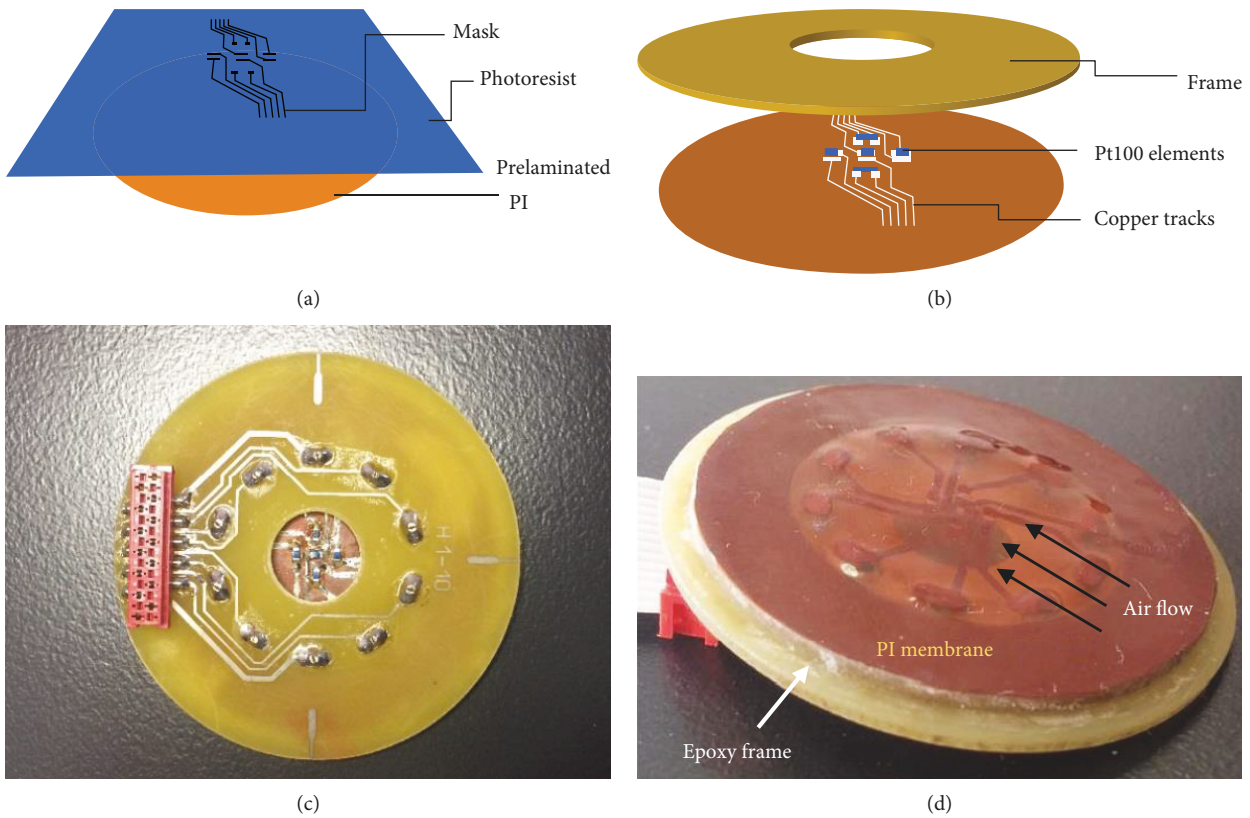

Figure 2: The sensor fabrication process. (a) Standard PCB photolithography was utilized for patterning copper onto the prelaminated Kapton film. (b) Thermistors were soldered, and the packaging was fitted. (c) The device's upper surface with the heater and the sensing elements and (d) the bottom surface which faces the flow channel.

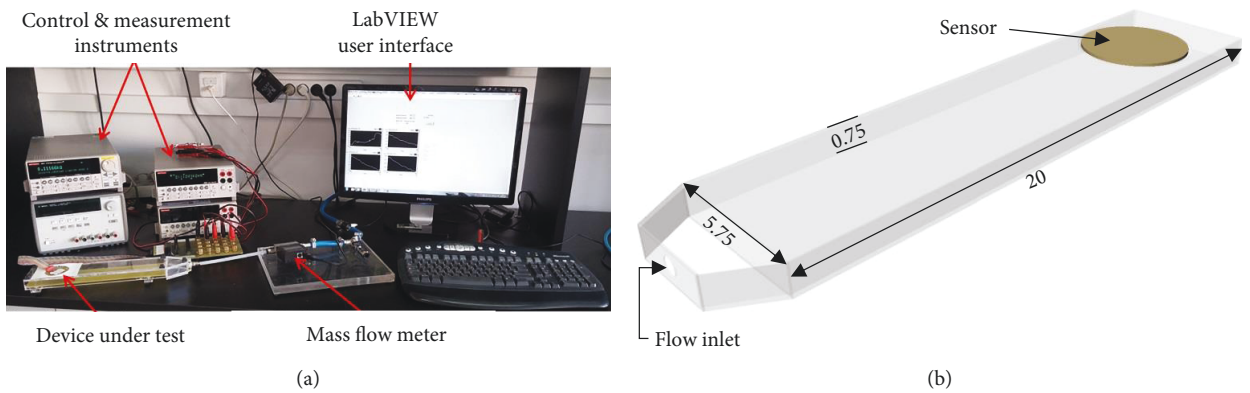

Figure 3: (a) The experimental setup. Arrows point the corresponding subcomponent of the setup. (b) Schematic of the measurement setup. The dimensions ensure laminar flow for the measurement flow rate range. Dimensions are in cm.

circular opening on the upper wall to fit the sensor under test. The channel has an orthogonal cross section with dimensions of 0.75 cm × 5.75 cm (Figure 3(b)). This apparatus allows for 360° rotation, while maintaining the surface of the sensor flat-aligned with the channel walls. Therefore, the initial flow vector is completely unaffected by the sensor angle and can be well defined, since the flow channel is effectively a simple rectangular pipe.

The setup is complemented by a controllable flow rate source, providing reference flow in the range of 0-25 standard liters per minute (SLPM), monitored alongside with fluid temperature by a precision Alicat M-series flow sensor. The corresponding Reynolds number does not exceed the value of 770; thus, laminar flow is maintained inside the flow channel. Power is applied to the heating element through a Keithley 2612 SourceMeter that simultaneously monitors the corresponding voltage/current, whereas the sensing elements' response is measured by a Keithley 2000 multimeter. All the electronic devices are connected to a PC through the LabVIEW software; thus, all the signals are monitored and controlled in real time. The corresponding data are also stored in a PC for further processing.

4. Results

4.1. Flow Rate Response. The sensor's response was evaluated in the region 0-25 SLPM under constant current (CC) and constant temperature (CT) mode utilizing the hot wire principle of operation, as depicted in Figure 4. In the first case, a constant current of 30 mA was supplied to the heating element, corresponding to approximately 120 mW under zero flow conditions, while in the second case, the heating element was kept at a constant operating point of 70°C by adjusting the applied power in order to compensate for the flow-induced temperature variations. Air flow with a constant temperature of 25°C was provided from a compressor, which was utilized prior to experiments until it reached a steady operating temperature.

As illustrated in Figure 4, both modes of operation result in a relatively high sensitivity in the specific flow range, with no visible saturation in the indicated flow values. However, it is obvious that the CT mode is a better choice for the determination of the flow rate since an improved sensitivity is obtained in the entire flow range under test. Moreover, a higher sensor response has been extracted, which is defined by the variation in heater power throughout the entire flow range. The specific response was $\Delta P = 12.6$ mW in the CT mode, compared to -2.89 mW in the CC mode for flow variation from 0 to 25 SLPM. For comparison purposes, both responses are shown in the same scale at the inset of Figure 4. Additionally, the CT mode presents the advantage of nonsaturated behavior in higher flow values, which cannot be shown in Figure 4, since the flow velocities under evaluation are comparatively low (maximum average fluid velocity 0.97 m/s).

4.2. Static-Dynamic Response. When referring to the time response of a flow sensor, there are two main categories: static and dynamic responses. The static time response can be obtained without flow by applying an electrical pulse to the heater and measuring the time required for the same heater (for the hot wire principle of operation) or for the nearby sensing element (for the deferential principle of operation) to reach a steady temperature. The dynamic time response can be estimated under flow, and it is defined from the time required for a sensor to reach a steady state under a sudden flow pulse. Given the fact that forming a step flow pulse is not trivial, in most of the cases in the literature, the term response time for flow sensors refers to the static time response.

For static response time determination of the present system, a current pulse of 30 mA was applied to the heater; thus, a time response in the order of 800 ms was extracted for the hot wire principle of operation.

For the evaluation of the sensor dynamic response, four sets of measurements were performed, from 10 to 25 SLPM with a step of 5 SLPM. In each initial flow velocity, pulses were created by changing the state of an on-off valve, which was connected in series to the flow tube. The response time of the valve was in the order of tenths of second (off: zero flow, on: set-point flow). In all the cases,

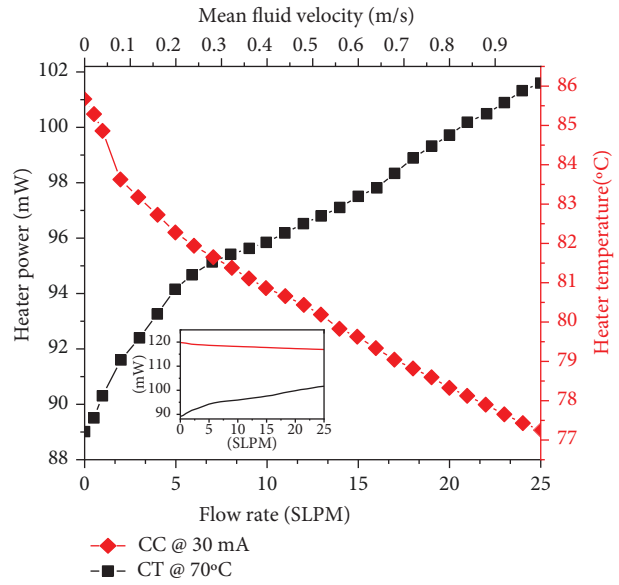

Figure 4: Heater power (CT mode, left y axis) and heater temperature (CC mode, right y axis) as a function of the applied flow. Inset: both modes' power response to the same flow range for comparison.

a constant current of 30 mA was supplied to the heater. The heater's signal was monitored in real time as well as the differential signal of two sensing elements, situated symmetrically in upstream and downstream positions with respect to the flow; referring to Figure 1, the flow was applied to y axis and the temperature difference was extracted from sensing elements R1-R3.

The results are illustrated in Figure 5, where the normalized resistance of the heater and the differential elements are presented as a function of time. For each case, normalization was performed according to equation (2), in order for the signals to be comparable; the valve state changes are clearly indicated by changing the monitored signals.

$$X_n = \frac{(X - X_{\min})}{(X_{\max} - X_{\min})}, \tag{2}$$

where $X_{\min}/X_{\max}$ is the heater minimum/maximum resistance (for the hot wire principle of operation) or minimum/maximum ΔR (for differential measurements).

Flow was provided by a generic air compressor; thus, small oscillations and signal drifting were observed, which induced fluctuation in the sensing element signal; more specifically, the differential signal was more sensitive to flow fluctuations, while heater's signal was slightly more immune. This difference in sensitivity can be observed in the response time extraction as well.

In order to define the dynamic response time for the specific device to flow alternation, we calculate the rise and fall time for the corresponding sensor responses to flow pulses in various flow values, as shown in Figure 6.

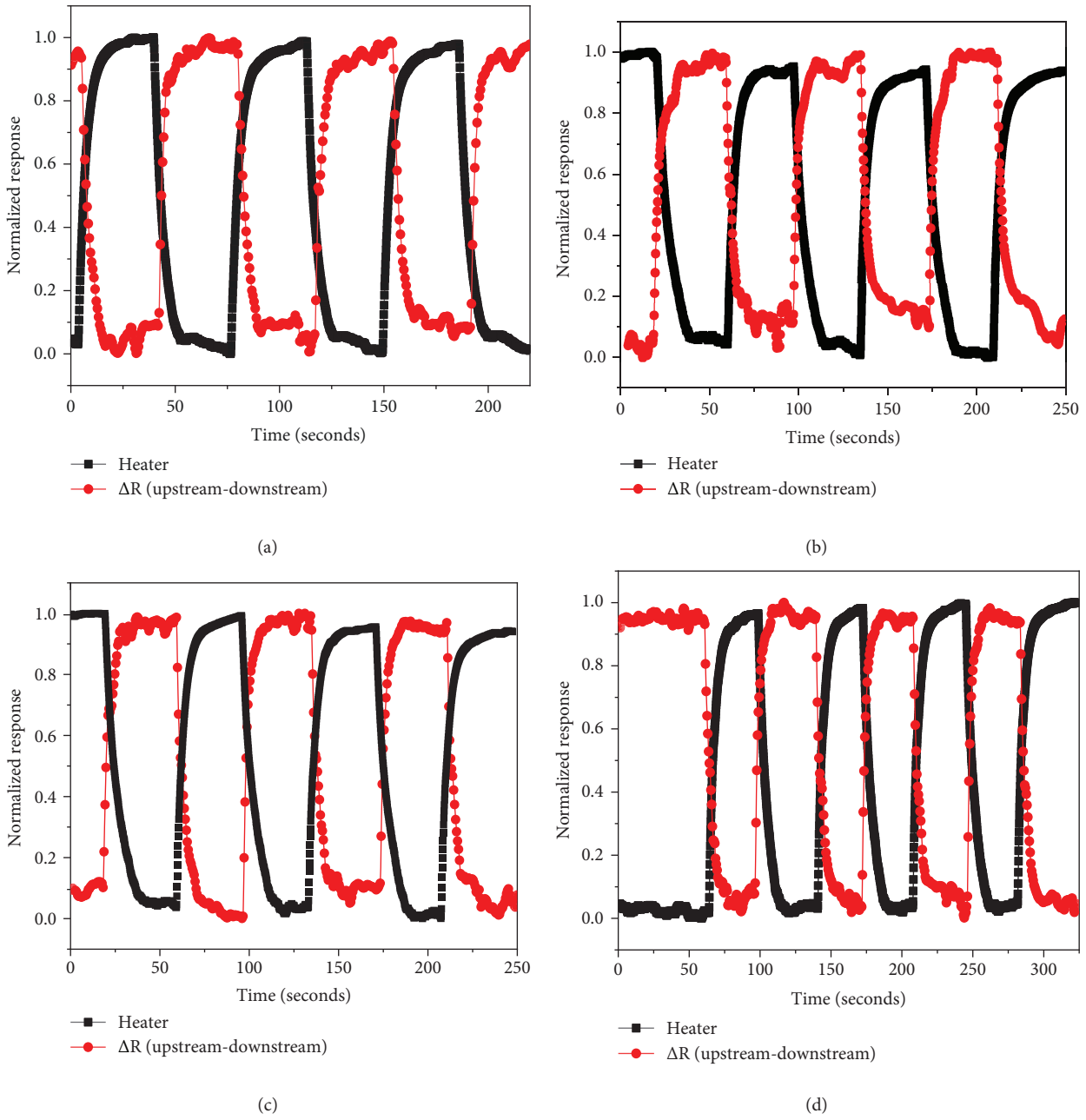

Figure 5: Normalized heater resistance (black square symbol) and upstream-downstream thermistors' normalized differential resistance (red circle symbol) response to flow pulses: (a) 10, (b) 15, (c) 20, and (d) 25 SLPM flow.

The sensor response as a function of time is presented for the (a) heater and (b) the differential element signal.

In each case, the corresponding response is presented during a valve change-state cycle. The dynamic response time is defined as the corresponding pulse rise (and fall) time, which is defined as the time needed for the signal to change between 10% and 90% of its final value, when flow is applied in the channel. For each calculation, an on-off alternation from Figure 5 was used, with a final value being the value used as maximum for signal normalization. Afterwards, a mean value of all the response times was calculated, which is the value indicated in black in Figures 6(a) and 6(b).

These dynamic response time values incorporate the time required by the setup to reach a steady flow (compressor, valve, and custom channel) as well as the proposed sensor's response to that flow.

4.3. Flow Direction Response. The aforementioned equation (1) can be simplified when the temperature dependence of Pt100 elements is taken into account. As mandated by the IEC60751 standard, the Pt100 sensing elements' resistance presents an effectively linear correlation with temperature for $T > 0^{\circ}$C and a small temperature variation; therefore, ΔT_x and ΔT_y in (1) can be substituted by $k\Delta R_x$ and $k\Delta R_y$, respectively, where ΔR represents the difference in resistance

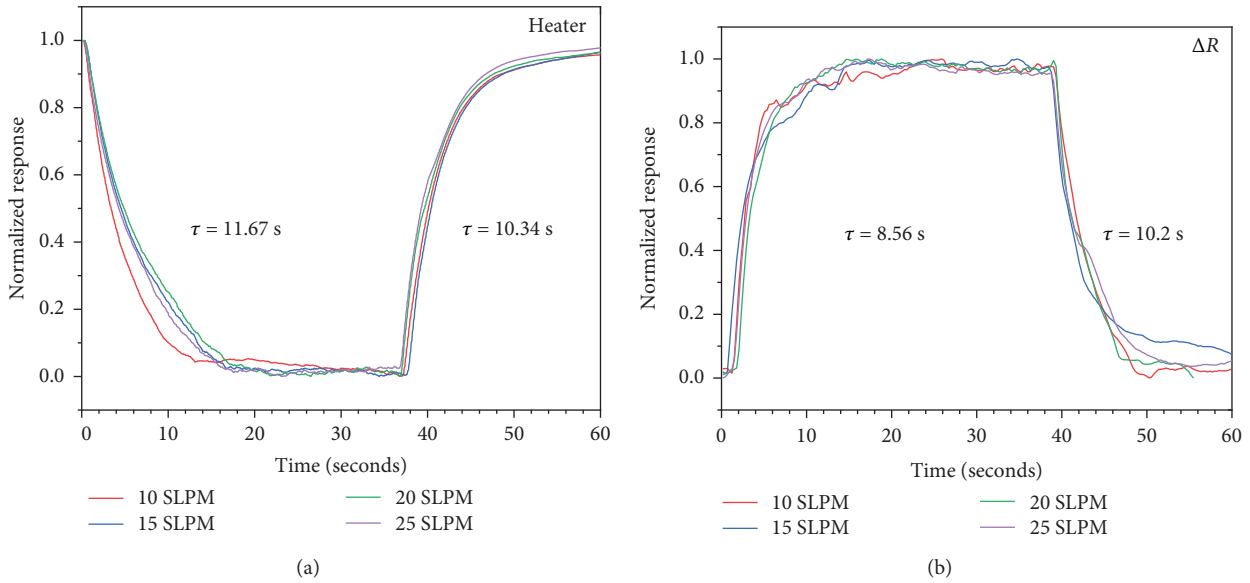

Figure 6: Calculation of 10-90% average response time from different flow rates: (a) heater's dynamic response and (b) differential elements (upstream-downstream to 0° flow) mean dynamic response.

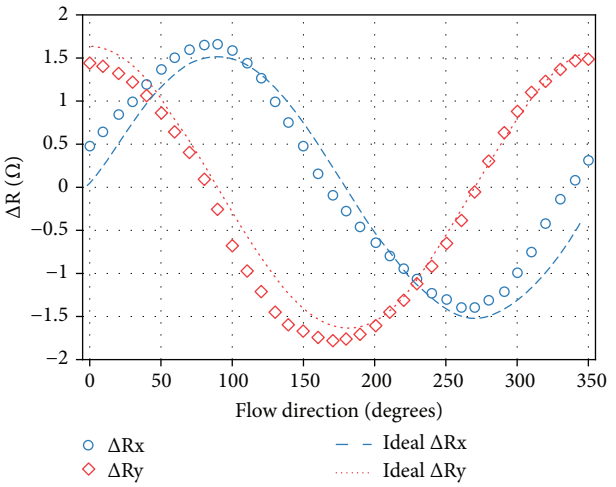

Figure 7: Raw differential data as a function of the flow angle. Dashed lines indicate ideal responses for each difference.

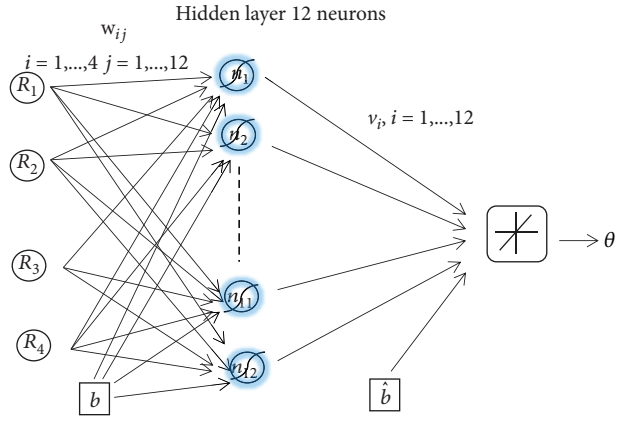

Figure 8: Structure of the neural network.

of the element pair along the x and y axes accordingly and k represents a constant factor, dominated by the TCR of the sensing element.

The device's response as a function of flow direction is presented in Figure 7, where the parameters ΔR_x and ΔR_y are plotted in respect to the flow angle; the entire range from 0 to 350 degrees is covered in 10 degree increments. A constant flow rate of 25 SLPM was applied during the directional response evaluation; the heater was operated at a constant 30 mA current (approx. 117 mW, 75°C).

Experimental results, shown in Figure 7, indicate that the sensor exhibits adequate sensitivity with respect to the flow direction. A phase difference and a small vertical offset are observed in comparison to ideal response curves; however, these systematic deviations can be attributed to slight asymmetries in the device layout and can be easily compensated by utilizing a suitable Artificial Neural Network.

5. Data Fusion

In order to improve the direction estimation, a single-layer back propagation neural network that correlates the four sensors' readouts to the angle of rotation was developed, i.e.,

$$f(R_1, R_2, R_3, R_4) = \theta \approx \left(\frac{\Delta T_y}{\Delta T_x}\right). \quad (3)$$

After extensive numerical tests, we have set the number of hidden neurons to 12 (Figure 8). This relatively small number of neurons has been proved effective as it gave very good results at considerably small computational costs. For the training of the neural network, we have

Table 1: Neural network results.

Method	Mean training epochs	Mean training error	Max training absolute error	Mean absolute error for best training	Root mean square error for best training	Indep. dataset mean absolute error for best training	Indep. dataset max absolute error for best training
Levenberg-Marquardt	5.4	2.9	0.32	0.09	0.13	2.7	11.0
Bayesian regulation	536.02	10.3	0.9	0.23	0.34	2.11	4.9
Fletcher-Powell conjugate gradient	6.6	9.8	6.8	2.46	1.8	2.98	7.3
BFGS quasi-Newton	7.9	11.3	8.5	4.18	3.67	4.45	11.03

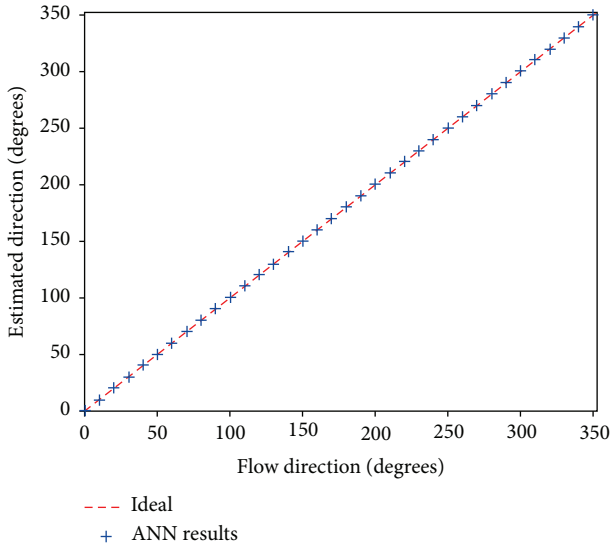

Figure 9: Estimated flow angle in comparison to ideal response.

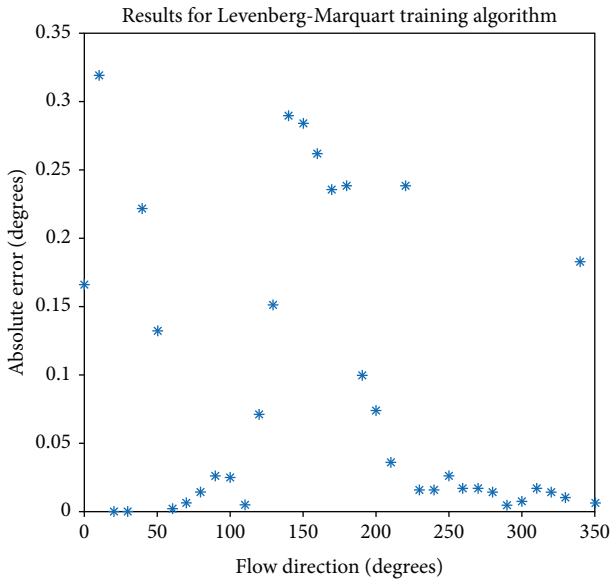

Figure 10: Absolute error values of the neural network as a function of the flow direction.

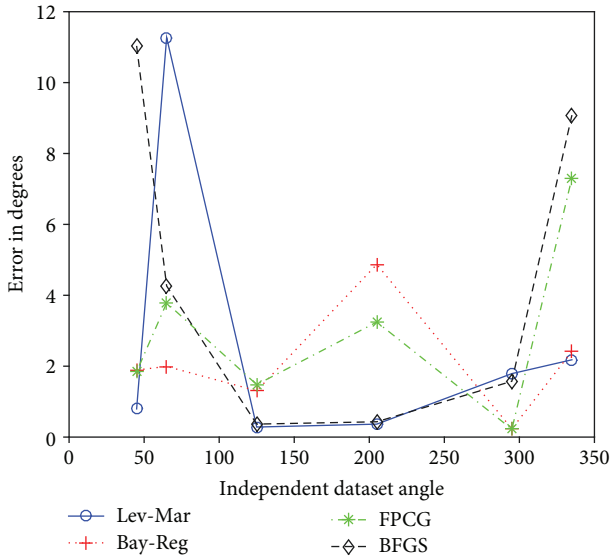

Figure 11: Error values of the neural network for the independent dataset.

tested four popular backpropagation algorithms [37–39]. The Levenberg-Marquardt method excels with fast convergence and relative cheap computational cost as it does not need to compute the Hessian matrix. This particular method is considered a standard methodology. The Bayesian regulation method was selected since it is generally considered suitable for small datasets like the one we have here. The Fletcher-Powell conjugate gradient method is the third choice and finally the classical BFGS quasi-Newton algorithm. All the tests were performed in MATLAB [40].

The experimental data, i.e., the four sensor's readouts from the experimental setup as described above, corresponding to a full rotation of the sensor from 0° to 350° at 10° per step were utilized for the construction of the neural network. Moreover, the original dataset has been split into three subsets in a percentage 70%, 15%, and 15%, namely, a training subset comprised of 25 data points, a validation subset consisting of 6 data points, and a testing subset comprised of 6 data points. The dataset under evaluation was taken for the flow rate of 25 SLPM. Similar evaluation can be performed for various flow directions in order to acquire the directional characteristics as a function of the flow rate, which is a subject for future work.

Table 2: 2D sensor review.

Flow range	Sensitivity	Static response time	Power consumption (mW)	2D accuracy	Reference
≤20 m/s	0.07 V/(m/s)	16 ms	—	—	[15]
0.025–0.2 m/s	30 mV/(m/s)	—	4	—	[16]
5–10 m/s	4.4 mV/(m/s)	A few seconds	50	5°	[17]
-0.4–0.4 SLPM	0.19 V W^{-1} m^{-1} s	10 ms	5.95	1.7°	[18]
-0.2–0.2 SLPM	1.9 V W^{-1} m^{-1} s	—	5	3.1°	
≤25 m/s	—	—	400		[19]
≤2 m/s	33.33 V/W/(m/s)	—	4	5°	[20]
≤5 m/s	12.99 V/W/(m/s)	10 ms	0.177	3.5°	[21]
0.2–9 m/s	1.2 $V^2/(m/s)^{0.5}$	<15 ms	160	0.96°	[28]
0-25 SLPM	12.6 mW/(m/s) (CT) -2.80 mW/(m/s) (CC)	0.8 s (CC mode)	CC mode: 120	2.7°	This work

In Table 1, we present the overall results. From the first three columns, we conclude that the trainings with the Levenberg-Marquardt method are the fastest, the mean of the errors is quite small, and it furnishes the best neural network. Bayesian regulation method proves to be very slow in the training procedure; the other two competitors, even if fast during training, do not perform satisfyingly.

The chosen neural network provides a very accurate direction estimation, as shown in Figure 9, resulting in a maximum absolute error of 0.32 degrees and a mean absolute error of 0.09 degrees; whereas the mean square error is 0.13 degrees. The overall error distribution is presented in Figure 10.

In order to further test the proposed neural network, an additional, independent dataset was used, corresponding to rotations of 45, 65, 125, 205, 295, and 335 degrees. It should be noted that these data points have not been involved at all in the ANN construction procedure. Figure 11 presents the performance of each tested ANN algorithm, assuming the independent dataset values for comparison. Among the backpropagation training algorithms, Levenberg-Marquardt and Bayesian regulation result to the lowest error values. However, the characteristics presented in Table 1 and corresponding discussion lead to the adaption of the Levenberg-Marquardt algorithm. For this methodology, the mean absolute error obtained is 2.7 degrees. It should be taken into consideration that inherent setup limitations (i.e., the angle setting resolution is 1 degree) are included in the overall achievable accuracy mentioned above.

In Table 2, a comparison with similar sensors found in literature is presented for reference. Although the proposed sensor is manufactured with low-end processes, it is evident that its performance is suitable for a wide range of 2D flow sensing applications, and its characteristics are comparable with state-of-the-art devices presented in the literature.

6. Conclusions

In this work, a thermal gas flow sensor for measuring two-dimensional flow was developed and evaluated in a constant current and constant temperature mode. A supplementary Artificial Neural Network was also developed in order to compensate for sensor asymmetries. In the proposed implementation, the flow is completely isolated from the active elements of the device. The flexible substrate allows for nonplanar installation; obtained measurements show promising results considering the low cost and complexity of the implementation; the measurable flow rate range extends from 0 up to more than 25 SLPM while the mean absolute error in direction estimation is 0.09 degrees within the training data and 2.7 degrees for a completely independent dataset. Further sensor development, including improvements on the layout and fabrication tolerances, is expected to provide a low-cost solution, especially for harsh environment applications that require measurement of low flow rates.

Data Availability

The data used to support the findings of this study are available from the corresponding author upon request.

Conflicts of Interest

The authors declare that there is no conflict of interest regarding the publication of this paper.

References

[1] S. D. Nguyen, I. Paprotny, P. K. Wright, and R. M. White, "MEMS capacitive flow sensor for natural gas pipelines," *Sensors and Actuators A: Physical*, vol. 231, pp. 28–34, 2015.

[2] E. van Doorn, B. Dhruva, K. R. Sreenivasan, and V. Cassella, "Statistics of wind direction and its increments," *Physics of Fluids*, vol. 12, no. 6, pp. 1529–1534, 2000.

[3] E. Gil, M. Gallart, P. Balsari, P. Marucco, M. P. Almajano, and J. Llop, "Influence of wind velocity and wind direction on measurements of spray drift potential of boom sprayers using drift test bench," *Agricultural and Forest Meteorology*, vol. 202, pp. 94–101, 2015.

[4] J. R. Platt, "Wind detection in a microcosm: ship/aircraft environment sensors," *IEEE Aerospace and Electronic Systems Magazine*, vol. 13, no. 2, pp. 26–33, 1998.

[5] C. Ghouila-Houri, Q. Gallas, E. Garnier et al., "High temperature gradient calorimetric wall shear stress micro-sensor for

flow separation detection," *Sensors and Actuators A: Physical*, vol. 266, pp. 232–241, 2017.

[6] M. Shikida, K. Yoshikawa, S. Iwai, and K. Sato, "Flexible flow sensor for large-scale air-conditioning network systems," *Sensors and Actuators A: Physical*, vol. 188, pp. 2–8, 2012.

[7] T. Glatzl, H. Steiner, F. Kohl, T. Sauter, and F. Keplinger, "Development of an air flow sensor for heating, ventilating, and air conditioning systems based on printed circuit board technology," *Sensors and Actuators A: Physical*, vol. 237, pp. 1–8, 2016.

[8] I. Abohela, N. Hamza, and S. Dudek, "Effect of roof shape, wind direction, building height and urban configuration on the energy yield and positioning of roof mounted wind turbines," *Renewable Energy*, vol. 50, pp. 1106–1118, 2013.

[9] T. Pennell, J. L. Yi, B. A. Kaufman, and S. Krishnamurthy, "Noninvasive measurement of cerebrospinal fluid flow using an ultrasonic transit time flow sensor: a preliminary study," *Journal of Neurosurgery: Pediatrics*, vol. 17, no. 3, pp. 270–277, 2016.

[10] S. Watanabe, Y. Hasegawa, M. Matsushima, T. Kawabe, and M. Shikida, "Micromachined tube type thermal flow sensor for adult-sized tracheal intubation tube," *Proceedings*, vol. 1, no. 4, p. 357, 2017.

[11] B. Abbasnejad, W. Thorby, A. Razmjou, D. Jin, M. Asadnia, and M. Ebrahimi Warkiani, "MEMS piezoresistive flow sensors for sleep apnea therapy," *Sensors and Actuators A: Physical*, vol. 279, pp. 577–585, 2018.

[12] R. Sawada, H. Nogami, R. Inoue, and E. Higurashi, "Blood flow sensor with built-in contact pressure and temperature sensor," in *2018 Symposium on Design, Test, Integration & Packaging of MEMS and MOEMS (DTIP)*, pp. 1–4, Roma, Italy, 2018.

[13] B. Tian, H. Li, N. Yang, Y. Zhao, P. Chen, and H. Liu, "A MEMS flow velocity sensor with low kinetic energy dissipation rate," *Sensor Review*, vol. 37, no. 3, pp. 247–256, 2017.

[14] J. Wang, W. Ding, L. Pan et al., "Self-powered wind sensor system for detecting wind speed and direction based on a triboelectric nanogenerator," *ACS Nano*, vol. 12, no. 4, pp. 3954–3963, 2018.

[15] K.-S. Shin, D.-S. Lee, S.-W. Song, and J. P. Jung, "Application of surface protective coating to enhance environment-withstanding property of the MEMS 2D wind direction and wind speed sensor," *Sensors*, vol. 17, no. 9, p. 2152, 2017.

[16] F. Keplinger, J. Kuntner, A. Jachimowicz, F. Kohl, and B. Jakoby, "Highly sensitive sensor for flow velocity and flow direction measurement," in *2006 5th IEEE Conference on Sensors*, pp. 1436–1439, Daegu, Korea, 2006.

[17] S. Kim, S. Kim, Y. Kim, S. Choi, and S. Park, "Design and fabrication of a flow sensor detecting flow direction and velocity,," in *TRANSDUCERS '03. 12th International Conference on Solid-State Sensors, Actuators and Microsystems. Digest of Technical Papers (Cat. No.03TH8664)*, pp. 1927–1930, Boston, MA, USA, 2003.

[18] J. Robadey, O. Paul, and H. Baltes, "Two-dimensional integrated gas flow sensors by CMOS IC technology," *Journal of Micromechanics and Microengineering*, vol. 5, no. 3, pp. 243–250, 1995.

[19] B. Chen, Y.-Q. Zhu, Z. Yi, M. Qin, and Q.-A. Huang, "Temperature effects on the wind direction measurement of 2D solid thermal wind sensors," *Sensors*, vol. 15, no. 12, pp. 29871–29881, 2015.

[20] P. Bruschi, M. Dei, and M. Piotto, "A low-power 2-D wind sensor based on integrated flow meters," *IEEE Sensors Journal*, vol. 9, no. 12, pp. 1688–1696, 2009.

[21] A. S. Cubukcu, E. Zernickel, U. Buerklin, and G. A. Urban, "A 2D thermal flow sensor with sub-mW power consumption," *Sensors and Actuators A: Physical*, vol. 163, no. 2, pp. 449–456, 2010.

[22] R.-Y. Que and R. Zhu, "A compact flexible thermal flow sensor for detecting two-dimensional flow vector," *IEEE Sensors Journal*, vol. 15, no. 3, pp. 1931–1936, 2015.

[23] J. H. Huijsing, J. P. Schuddemat, and W. Verhoef, "Monolithic integrated direction-sensitive flow sensor," *IEEE Transactions on Electron Devices*, vol. 29, no. 1, pp. 133–136, 1982.

[24] N.-T. Nguyen, "A novel wind sensor concept based on thermal image measurement using a temperature sensor array," *Sensors and Actuators A: Physical*, vol. 110, no. 1–3, pp. 323–327, 2004.

[25] M. Yarali and S. K. Khanna, "Microfabrication of a variable range and multi-directionally sensitive thermal flow sensor," *Sensors and Actuators A: Physical*, vol. 220, pp. 159–167, 2014.

[26] B. W. van Oudheusden and J. H. Huijsing, "Integrated silicon flow-direction sensor," *Sensors and Actuators*, vol. 16, no. 1-2, pp. 109–119, 1989.

[27] K. A. A. Makinwa and J. H. Huijsing, "A smart wind sensor using thermal sigma-delta modulation techniques," *Sensors and Actuators A: Physical*, vol. 97-98, pp. 15–20, 2002.

[28] R. Que and R. Zhu, "A two-dimensional flow sensor with integrated micro thermal sensing elements and a back propagation neural network," *Sensors*, vol. 14, no. 1, pp. 564–574, 2014.

[29] R. Zhu, R. Que, and P. Liu, "Flexible micro flow sensor for micro aerial vehicles," *Frontiers of Mechanical Engineering*, vol. 12, no. 4, pp. 539–545, 2017.

[30] T. A. Johansen, A. Cristofaro, K. Sorensen, J. M. Hansen, and T. I. Fossen, "On estimation of wind velocity, angle-of-attack and sideslip angle of small UAVs using standard sensors," in *2015 International Conference on Unmanned Aircraft Systems (ICUAS)*, pp. 510–519, Denver, CO, USA, 2015.

[31] P. Bruschi and M. Piotto, "Determination of the wind speed and direction by means of fluidic-domain signal processing," *IEEE Sensors Journal*, vol. 18, no. 3, pp. 985–994, 2018.

[32] M. Corno, S. Formentin, and S. M. Savaresi, "Data-driven online speed optimization in autonomous sailboats," *IEEE Transactions on Intelligent Transportation Systems*, vol. 17, no. 3, pp. 762–771, 2016.

[33] S.-H. Choa, "Reliability of MEMS packaging: vacuum maintenance and packaging induced stress," *Microsystem Technologies*, vol. 11, no. 11, pp. 1187–1196, 2005.

[34] Y. Mitsunari, Y. Hasegawa, M. Matsushima, T. Kawabe, and M. Shikida, "Development of small-footprint thermal sensor detecting airflow at mouth in baby," *Proceedings*, vol. 1, no. 4, p. 359, 2017.

[35] C. Ghouila-Houri, Q. Gallas, E. Garnier et al., "Wall shear stress calorimetric micro-sensor designed for flow separation detection and active flow control," *Proceedings*, vol. 1, no. 4, p. 376, 2017.

[36] A. Moschos, D. Barmpakos, and G. Kaltsas, "A multi-directional thermal flow sensor fabricated on flexible substrate," in *SENSORDEVICES 2015: The Sixth International Conference on Sensor Device Technologies and Applications*, p. 68, Venice, Italy, 2015.

[37] J. Nazari and O. K. Ersoy, "Implementation of back-propagation neural networks with MatLab," ECE Technical Reports Paper 275, 1992.

[38] Y. Chauvin and D. E. Rumelhart, *Backpropagation: Theory, Architectures, and Applications*, Psychology Press, 2013.

[39] R. Fletcher, *Practical Methods of Optimization*, Wiley, 1987.

[40] *MATLAB and Neural Network Toolbox Release*, The MathWorks, Inc, Natick, MA, USA, 2014.